MODEL OF MAGNETICALLY ENHANCED, CAPACITIVE RF DISCHARGES

by

M.A. Lieberman, A.J. Lichtenberg, and S.E. Savas

Memorandum No. UCB/ERL M90/58

2 July 1990

MODEL OF MAGNETICALLY ENHANCED, CAPACITIVE RF DISCHARGES

by

M.A. Lieberman, A.J. Lichtenberg, and S.E. Savas

Memorandum No. UCB/ERL M90/58

2 July 1990

ELECTRONICS RESEARCH LABORATORY

College of Engineering
University of California, Berkeley
94720

MODEL OF MAGNETICALLY ENHANCED, CAPACITIVE RF DISCHARGES

by

M.A. Lieberman, A.J. Lichtenberg, and S.E. Savas

Memorandum No. UCB/ERL M90/58

2 July 1990

ELECTRONICS RESEARCH LABORATORY

College of Engineering
University of California, Berkeley
94720

ABSTRACT

Magnetically enhanced, capacitive r.f. discharges (so-called r.f. magnetrons or MERIE discharges) are playing an increasing role in thin film etching for integrated circuit processing. In these discharges, a weak d.c. magnetic field is imposed lying parallel to the powered electrode surface. We determine the r.f. power transferred to the discharge electrons by the oscillating electron sheath in the presence of the magnetic field. Using this along with particle and energy conservation, we obtain discharge parameters such as the ion flux and ion bombarding energy at the powered electrode as functions of pressure, r.f. power, and magnetic field.

I. Introduction

R.F. discharges are widely used in the semiconductor industry for etching and sputtering processes; moreover, their use has become critical for VLSI circuit production[1–2]. Magnetically enhanced r.f. discharges (so-called r.f. magnetrons or MERIE configurations) are playing an increasing role in processing as feature sizes shrink. Although many phenomena occurring in r.f. plasma discharges have been studied during the past years[3–7], discharge models are just now becoming capable of predicting the plasma state of an asymmetric (unequal powered and grounded electrode areas) *nonmagnetized*, r.f. discharge for given values of controllable parameters[8–10]. Such models can be used to predict the main discharge parameters from a processing point of view, such as the ion bombarding energy and ion fluxes to the powered electrode[8–10]. In this work, we develop such a model for low pressure magnetically enhanced discharges. Because of the added complexity of the crossed B-field, a simplifying assumption that the density is uniform in the discharge is employed[5]. A model using this assumption, while not quantitatively correct, is of value in understanding the principles of discharge operation and the scaling of various discharge characteristics.

Figure 1 shows the basic geometry of a plane parallel, magnetically enhanced discharge. Gas at pressure p fills the region between two electrodes of area A separated by a distance l. When a voltage V_{rf} at frequency ω is applied, the gas breaks down, forming a processing plasma. Magnetic enhancement is obtained by applying a weak d.c. magnetic field B_0 having field lines lying parallel to the powered electrode surface where the wafers are placed. For typical discharge operation, the system is driven at 13.56 MHz with V_{rf} ~ 50–500 V, p ~ 3–100 mTorr, B_0 ~ 50–300 G, and l ~ 3–30 cm.

In Sec. II, we develop the basic plasma and sheath model equations for a homogeneous magnetically enhanced discharge in which the ion density is assumed to be uniform (the homogeneous model). In Sec. III, we extend the basic theory of electron heating by the oscillating

r.f. sheaths in an unmagnetized discharge to the case of a homogeneous sheath model with magnetic enhancement, and we show that the magnetic field enhances the transfer of r.f. power by the oscillating sheath to the discharge electrons. In Sec. IV, we incorporate the enhancement along with particle and energy conservation to determine the discharge equilibrium and such parameters as the ion flux and ion bombarding energy at the powered electrode as functions of the discharge pressure, r.f. power, and magnetic field. In Sec. V, we present numerical solutions of the analytical model and compare these with experiments.

II. Homogeneous Model

We assume a uniform ion density n confined between infinite parallel plates located at $x = 0$ and $x = l$. A uniform magnetic field B is oriented along the z direction. A uniform sinusoidal current density

$$J_x(t) = \mathrm{Re} J_0 e^{j\omega t} = J_0 \cos \omega t \tag{1}$$

flows in the x direction. The current densities in the y and z directions are assumed to vanish. This models perfectly insulating walls in the y and z directions for a discharge with finite transverse dimensions.

In the plasma, the current density is related to the electric field vector through the dielectric tensor. Letting $J_\alpha(t) = \mathrm{Re}\tilde{J}_\alpha e^{j\omega t}$ and $E_\alpha(t) = \mathrm{Re}\tilde{E}_\alpha e^{j\omega t}$, where $\alpha = x$, y, or z and the tilde denotes the complex amplitude, we obtain

$$\begin{bmatrix} \tilde{J}_x \\ \tilde{J}_y \\ \tilde{J}_z \end{bmatrix} = j\omega\varepsilon_0 \begin{bmatrix} K_\perp & -K_\times & 0 \\ K_\times & K_\perp & 0 \\ 0 & 0 & K_{||} \end{bmatrix} \begin{bmatrix} \tilde{E}_x \\ \tilde{E}_y \\ \tilde{E}_z \end{bmatrix}, \tag{2}$$

where the complex tensor elements are given by

$$K_\perp = (K_l + K_r)/2, \qquad K_\times = j(K_l - K_r)/2, \tag{3}$$

$$K_{r,l} = 1 - \frac{\omega_{pe}^2}{\omega(\omega \pm \omega_{ce} - j\nu_e)}, \tag{4}$$

$$K_{\|} = 1 - \frac{\omega_{pe}^2}{\omega(\omega - j\nu_e)} \ . \tag{5}$$

Setting $\tilde{J}_x = J_0$ and $\tilde{J}_y = \tilde{J}_z = 0$ and solving (2), we obtain $\tilde{E}_z = 0$,

$$\tilde{E}_y = -\tilde{E}_x K_\times / K_\perp \ , \tag{6}$$

and

$$\tilde{E}_x = [j\omega\varepsilon_0(K_\perp + K_\times^2/K_\perp)]^{-1} J_0 \ . \tag{7}$$

In the sheath region a (see Fig. 1), the x-component of the electric field is found by integrating Poisson's equation to obtain

$$E_{xa}(x,t) = en(x - s_a(t))/\varepsilon_0 + E_x(t) \ , \tag{8}$$

where $E_x(t)$ is the field in the plasma, and we have chosen $E_{xa} = E_x$ at the instantaneous position of the sheath edge $x = s_a$ because the discharge cannot support a surface charge at the plasma-sheath interface. Equating the displacement current flowing across the sheath to J_x, we obtain

$$J_x(t) = \varepsilon_0 \partial E_{sa}/\partial t = -en\,\partial s_a/\partial t + \varepsilon_0 \partial E_x/\partial t \ . \tag{9}$$

Letting

$$s_a(t) = s_0 + \mathrm{Re}\,\tilde{s}\ e^{j\omega t} \tag{10}$$

and inserting this into (9), we find

$$J_0 = -enj\omega\tilde{s} + j\omega\varepsilon_0\tilde{E}_x \ .$$

Inserting $\tilde{E}_x$ from (7) into this expression yields $\tilde{s}$ as a function of J_0:

$$\tilde{s} = (j\omega en)^{-1}[(K_\perp + K_\times^2/K_\perp)^{-1} - 1]\, J_0 \tag{11}$$

The time average conduction current flowing to plate a is assumed to vanish. There is a steady flow of ions to the plate, given by

$$\bar{J}_i = enu_B \ , \tag{12}$$

where $u_B = (eT_e/m_i)^{1/2}$ is the Bohm velocity, T_e is in units of volts, and m_i is the ion mass. The sheath thickness must therefore collapse to zero at some time during the rf cycle in order to transfer electrons to the plate. This condition sets

$$|\tilde{s}| = s_0 \ . \tag{13}$$

Similarly, there is a cross field oscillation of the plasma given by

$$0 = -enj\omega\tilde{s}_y + j\omega\varepsilon_0\tilde{E}_y \ , \tag{14}$$

where E_y is found from (6) and $\tilde{s}_y$ is the complex amplitude of the y-oscillation.

Integrating the electric field (8) from 0 to s_a, we obtain the electrode-plasma voltage

$$V_{ap}(t) = -ens_a^2/2\varepsilon_0 + E_x s_a \ . \tag{15}$$

For this symmetric discharge, the sheath at electrode b oscillates 180° out of phase with the sheath at electrode a. Hence, from (10), we find

$$s_b(t) = s_0 - \mathrm{Re}\,\tilde{s}\, e^{j\omega t} \ . \tag{16}$$

From this expression, we obtain

$$V_{bp}(t) = -ens_b^2/2\varepsilon_0 - E_x s_b \ . \tag{17}$$

The voltage drop across the two sheaths is

$$V_{sh}(t) = V_{ap} - V_{bp} = -en(s_a - s_b)(s_a + s_b) + E_x(s_a + s_b) \ . \tag{18}$$

Using (10) and (16) in (18), we obtain

$$V_{sh}(t) = -(2ens_0/\varepsilon_0)\,\mathrm{Re}\,\tilde{s}\, e^{j\omega t} + 2s_0E_x(t) \ . \tag{19}$$

Since E_x is harmonic in time, V_{sh} is harmonic in time with complex amplitude

$$\tilde{V}_{sh} = -2ens_0\tilde{s}/\varepsilon_0 + 2s_0\tilde{E}_x \ . \tag{20}$$

Adding to this the voltage drop $\tilde{E}_x d$ across the plasma, where $d = l - 2s_0$ is the bulk plasma thickness, we obtain the complex amplitude of the total discharge voltage

$$\tilde{V}_{rf} = -2\,ens_0\tilde{s}/\varepsilon_0 + \tilde{E}_x l \ . \tag{21}$$

Time averaging (15), we obtain the dc voltage across a single sheath:

$$\overline{V}_{pa} = \frac{3\,ens_0^2}{4\varepsilon_0} + \frac{1}{2}\mathrm{Re}\,\tilde{s}\tilde{E}_x^* \ , \tag{22}$$

which is the ion bombarding energy at the electrode.

The field equations must be coupled with particle and energy conservation in order to determine the discharge parameters. We do this in Sec. IV, after first determining the electron heating by the oscillating rf sheaths.

III. Sheath Heating

In a previous study[6], the dynamics for a self-consistent, collisionless sheath driven by a sinusoidal r.f. current source was obtained. It was shown that electrons could be heated by the oscillating sheath. An electron that is reflected from a moving sheath experiences a change of energy. If the sheath moves toward the electron, then the energy increases; if the sheath moves away, then the energy decreases. For an oscillating sheath, some electrons gain energy and others lose energy. However, averaging over an oscillation period, the net effect is an energy gain, corresponding to a power transfer due to *single collisions* of electrons with the moving sheath. The power transfer is obtained as a first order effect of the unperturbed sheath motion; i.e., the zero order sheath motion is taken to be purely capacitive (lossless)[6]. For weak magnetic fields, we argue that the zero order sheath motion remains unchanged, but that the first order calculation of the heating must be modified due to *multiple correlated collisions* of electrons with the moving sheath.

If u is the parallel velocity (along z) of an incident electron at the electron sheath edge

$s_a(t)$ and $u_s(t)$ is the sheath velocity, then the reflected electron has a velocity $u_r = -u + 2\Delta u$, where $2\Delta u(t)$ is the total velocity change of an electron that first hits the sheath at time t, due to the accumulation of subsequent multiple correlated sheath collisions. We let $f_s(u,t)$ be the electron velocity distribution at s, normalized so that

$$\int_{-\infty}^{\infty} f_s(u,t)\,du = n \ , \tag{23}$$

where n is the uniform ion density in the sheath. Assuming a Maxwellian distribution, the electron flux Γ_e incident on the sheath is

$$\Gamma_e = \int_0^{\infty} u f_s(u,t)\,du = \frac{1}{4} n u_e \ , \tag{24}$$

where $u_e = (8eT_e/\pi m)^{1/2}$ is the mean electron speed.

To determine the power transferred to the electrons, we note that in a time interval dt and for a speed interval du, the number of electrons per unit area that collide with the sheath is given by $(u - u_s) f_s(u,t)\,du\,dt$. This results in a power transfer dP per unit area

$$dP = \frac{1}{2} m(u_r^2 - u^2)(u - u_s) f_s(u,t)\,du. \tag{25}$$

Using $u_r = -u + 2\Delta u$ and integrating over all incident velocities, we obtain

$$P = -2m \int_{u_s}^{\infty} \Delta u(\Delta u - u)(u - u_s) f_s(u,t)\,du \ . \tag{26}$$

To determine f_s, we first note that the sheath is oscillating because the electrons in the plasma are oscillating in response to a time-varying electric field. If the velocity distribution function within the plasma in the absence of the electric field is a Maxwellian $g_0(u)$, then the distribution within the plasma is $f_0(u,t) = g_0(u - u_s)$, where, differentiating (10),

$$u_s(t) = \mathrm{Re}\,\tilde{u}_s\, e^{j\omega t} \ , \tag{27}$$

is the time-varying oscillation velocity of the plasma electrons, with $\tilde{u}_s = \omega\tilde{s}$. Inserting f_s into (26) and transforming to a new variable $u' = u - u_s$, we obtain

$$P(t) = -2m\int_0^\infty \Delta u n [u'^2 - u'(\Delta u - u_s)] g_0(u')\, du' . \tag{28}$$

Averaging (28) over $\phi = \omega t$ and noting that Δu and u_s are odd functions of ϕ, the first term in (28) averages to zero and we obtain

$$P_{stoc} = 2m\Gamma_e \langle \Delta u\, (\Delta u - u_s) \rangle_\phi . \tag{29}$$

For a homogeneous sheath model in the absence of a magnetic field, the change $2\Delta u$ in electron velocity for one collision with the oscillating sheath is $2\Delta u = 2u_s$. Inserting this result in (29), we see that $P_{stoc} = 0$, a result obtained for the homogeneous model in reference 6. To determine Δu for the multiple sheath collisions in a magnetically enhanced discharge, we let $2u_s(\omega t)$ be the change in electron velocity for a single collision with the sheath at time t. For a slowly moving sheath, successive collisions take place at time intervals of $\Delta t = \pi/\omega_{ce}$, where $\omega_{ce} = eB/m$ is the electron gyration frequency. These collisions result in coherent energy gain. However, the coherent energy gain is terminated by electron collisions with neutral gas atoms. Hence we can write

$$\Delta u = u_s(\omega t) + \sum_{k=1}^{\infty} u_s(\omega t + k\omega\Delta t)\, e^{-k\nu_e \Delta t} , \tag{30}$$

where ν_e is the electron-neutral scattering frequency. The exponential factor in (30) gives the fraction of electrons that have not collided with neutral gas atoms after a time $k\Delta t$. We are interested in the regime $\omega, \nu_e \ll \omega_{ce}$, so we can convert the sum to an integral, which yields

$$\Delta u = u_s + \frac{\omega_{ce}}{\pi\omega}\int_0^\infty u_s(\phi + \phi')\, e^{-\nu_e \phi'/\omega} d\phi' . \tag{31}$$

Substituting (27) into (31) and integrating, we obtain

$$\Delta u(\phi) = \mathrm{Re}\,\tilde{u}_s \left[1 + \frac{\omega_{ce}}{\pi(\nu_e - j\omega)}\right] e^{j\phi} . \tag{32}$$

Inserting this expression into (29) and averaging, we obtain the time average power per unit area delivered to the electrons by the oscillating sheath:

$$P_{stoc} = \frac{1}{4} mnu_e |\tilde{u}_s|^2 \frac{\omega_{ce}}{\pi(\nu_e^2 + \omega^2)} (\nu_e + \frac{\omega_{ce}}{\pi}) . \tag{33}$$

Although not valid in the regime $\omega_{ce} \ll \omega, \nu_e$, we note that (33) yields the correct limit for the homogeneous sheath: $P_{stoc} \to 0$ as $\omega_{ce} \to 0$.

IV. Discharge Equilibrium

Equating the particle flux lost to the electrodes to the particle generation in the discharge yields

$$2nu_B = nNK_{iz}d , \tag{34}$$

where $u_B = (eT_e/m_i)^{1/2}$ is the ion velocity at the ion sheath edge $x = 2s_0$, N is the neutral argon density, and $K_{iz}(T_e)$ is the ionization rate constant. Solving (34), we find

$$\frac{K_{iz}}{2u_B} = \frac{1}{Nd} . \tag{35}$$

For a given Nd, (35) can be solved numerically to determine T_e. Since $s_0 \ll l$, we can put $d \approx l$ in (35) with little error.

The electron power balance in the discharge can be written as

$$P_{ohm} + 2P_{stoc} = 2enu_B(\mathcal{E}_L + \mathcal{E}_e) \equiv P_{el} , \tag{36}$$

where $P_{ohm} = \frac{1}{2}\mathrm{Re}\,\tilde{E}_x J_0 d$ is the time average ohmic power per unit area, P_{stoc} is the sheath heating given by (33), $\mathcal{E}_L(T_e)$ is the electron energy loss per electron-ion pair created in the discharge due to ionization, excitation and elastic scattering of electrons with argon atoms, and $\mathcal{E}_e \approx 2T_e$ is the mean kinetic energy of lost electrons. The total power per unit area absorbed

by the discharge is

$$P_{rf} = 2\,enu_B(\mathcal{E}_L + \mathcal{E}_e + \bar{V}_{pa})\,, \tag{37}$$

where $\bar{V}_{pa}$ given by (22) is the ion bombarding energy. Eliminating $\tilde{E}_x$ from P_{ohm} and $|\tilde{u}_s|^2$ from P_{stoc} in terms of J_0, then the left hand side of (36) is proportional to J_0^2. Similarly eliminating $\tilde{s}$ and $\tilde{E}_x$ in favor of J_0 in (22) yields $\bar{V}_{pa} \propto J_0^2$. Hence solving (36) for J_0^2 as a function of n and inserting this into (37), we obtain a single equation that can be solved numerically to determine n for a given P_{rf}. Equation (36) then yields J_0, and the complex amplitudes $\tilde{E}_x$, $\tilde{E}_y$, $\tilde{s}$, $\tilde{s}_y$, $\tilde{V}_{rf}$, and the ion bombarding energy $\bar{V}_{pa}$ then follow from the results in Sec. II.

The magnetic field has two main effects on the discharge equilibrium: (1) The stochastic heating is proportional to B_0^2 and dominates the ohmic heating at low pressures and high magnetic fields. (2) A significant fraction of the total rf discharge voltage can be dropped across the bulk plasma at low powers and high magnetic fields.

If the bulk plasma voltage is small, then we can estimate the scaling of the equilibrium with P_{rf} and B_0 in various regimes as follows: We first note by current continuity that $J_0 \propto n\tilde{u}_s \propto ns_0$. Since the sheaths are capacitive, $J_0 \propto V_{rf}/s_0$. Hence it follows that $n \propto V_{rf}/s_0^2$. Using this result in (33), we obtain the scaling of the stochastic heating power $P_{stoc} \propto B_0^2 V_{rf}$ for $\omega_{ce} \gg \omega, \nu_e$. Similarly scaling the ohmic power yields $P_{ohm} \propto V_{rf}^{1/2}$. The power balance equations (36) and (37) can then be evaluated in the four limiting cases, depending on whether stochastic heating dominates ohmic heating and on whether ion energy losses dominate electron energy losses ($\bar{V}_{pa} \gg \mathcal{E}_L + \mathcal{E}_e$). The results are:

(a) Stochastic heating and ion energy losses dominate. Then $V_{rf} \propto P_{rf}^{1/2}/B_0$, $n \propto P_{rf}^{1/2}B_0$, $s_0 \propto B_0^{-1}$, and $P_{stoc} \propto P_{rf}^{1/2}B_0$.

(b) Stochastic heating and electron energy losses dominate. Then $V_{rf} \propto P_{rf}/B_0^2$, $n \propto P_{rf}$,

$s_0 \propto B_0^{-1}$, and $P_{stoc} \propto P_{rf}$.

(c) Ohmic heating and ion energy losses dominate. Then $V_{rf} \propto P_{rf}^{2/3}$, $n \propto P_{rf}^{1/3}$, $s_0 \propto P_{rf}^{1/6}$, and $P_{ohm} \propto P_{rf}^{1/3}$.

(d) Ohmic heating and electron energy losses dominate. Then $V_{rf} \propto P_{rf}^{2}$, $n \propto P_{rf}$, $s_0 \propto P_{rf}^{1/2}$, and $P_{ohm} \propto P_{rf}$.

If the bulk plasma voltage drop dominates the sheath drop, then different scalings are seen. In this regime we can consider the case:

(e) Stochastic heating and electron energy losses dominate. Then the power balance equations (36) and (37) yield $n \propto P_{rf}$ and $J \propto P_{rf}/B_0$ respectively. From (7), with $K_\perp - 1 \ll K_x$, we obtain the scaling $J \propto K_x^2 E_x$. Using $E_x \propto V_{rf}$ and $K_x \propto n/B_0$, we find $V_{rf} \propto (P_{rf} B_0)^{-1}$.

V. Numerical and Experimental Results

Figure 2 shows the momentum transfer rate constant K_m and the ionization rate constant K_{iz}, and Fig. 3 shows the energy loss ε_L per electron-ion pair created used in the numerical calculations that follow[8]. The energy losses include ionization, electronic excitation, and elastic scattering of electrons with neutral argon atoms.

Figure 4 shows the numerically determined solutions for V_{rf}, n, s_0, and P_{stoc} versus P_{rf} with B_0 as a parameter for a 3 mTorr discharge with l = 10 cm and f = 10 MHz. For this low pressure, stochastic heating dominates even at the lowest value of $B_0 = 10$ G. For $B_0 \leq 100$ G, the ion energy losses dominate and the scalings of case (a) are seen in the numerical results; e.g., the solid line in Fig. 4b shows $n \propto P_{rf}^{1/2}$ and the solid line in Fig. 4d shows $P_{stoc} \propto P_{rf}^{1/2}$. For $B_0 \geq 100$ G, the voltage drops sufficiently that the scalings of case (b) are observed; e.g., the dashed lines in Figs. 4a, b, and d. At the extreme value of $B_0 = 1000$ G and for low rf powers, the bulk plasma voltage drop dominates and we observe the scalings of case

(e); e.g., $V_{rf} \propto P_{rf}^{-1}$, as shown by the dot-dashed line in Fig. 4a. We also see that the discharge displays a form of resonant behavior, with V_{rf} having a minimum value at $P_{rf} \approx 500$ W/m^2.

Figure 5 shows the numerical solutions for V_{rf} and n at 100 mTorr, where ohmic heating dominates for $B_0 \leq 300$ G. For these magnetic fields, ion energy losses dominate at the highest powers and we see the scalings of V_{rf}, n, s_0 and J_0 described by case (c). For the highest magnetic field, we again see the effect of a series resonance.

Measurements were made in a commercial etch chamber (Applied Materials PE 5000) in argon at 13.56 MHz to compare with the model. The measurements show a surprising degree of agreement with the model in the values of the d.c. sheath voltage and the plasma density over the range of pressures, powers, and magnetic fields measured. In the experiment, the d.c. bias voltage $V_{bias} = \overline{V}_{pa} - \overline{V}_{pb}$ was measured. Since the discharge is strongly asymmetric in this commercial etch chamber, (the powered electrode area is much smaller than the grounded electrode area), $\overline{V}_{pb} \ll \overline{V}_{pa}$. Hence, the measured value of V_{bias} is compared with the model result for $\overline{V}_{pa}$. The plasma density n was measured approximately 3 cm in front of the 200 cm^2 powered electrode using a high impedance (at 13.56 MHz) Langmuir probe consisting of a tungsten wire having a radius $r_w = 0.013$ cm and a length $l_w = 0.6$ cm. The ion saturation current I_{sat} at probe biases V_w of -50 and -100 volts were measured and related to the ion density n and the plasma potential V_p by the expression:

$$I_{sat} = enr_w l_w [8e(V_p - V_w)/m_i]^{1/2} , \tag{38}$$

which is obtained from the Laframboise probe theory[11] and is valid for $r_w/\lambda_D \leq 2$, where λ_D is the electron Debye length. This condition is well met for our measurements. Solving (38) simultaneously for both probe biases, we obtain an estimate of n and V_p. The plasma potentials were in the range of 10-50 volts.

In Fig. 6, we compare the experimental measurements of V_{bias} with the numerical results for $\bar{V}_{pa}$ at three different pressures of 100, 30 and 10 mTorr, three different magnetic fields of 10, 30 and 100 gauss, and three different power densities of 0.25, 0.5 and 1.0 W/cm^2. We note (Fig. 6a) that the measured values (points) are within 10 percent of the model predictions (solid lines) at 100 mTorr and have almost exactly the same dependence on P_{rf}. There is as much as a 25 percent deviation in the 30 mTorr cases (Fig. 6b), but again the power scaling is quite accurate. At 10 mTorr (Fig. 6c), there is a larger discrepancy, but again very close power scaling.

The ion densities in Fig. 7 are seen to scale with power closely to the model predictions for most cases and are within a factor of two of the measured values for all cases. The major exception to the proper scaling seems to be the case of 100 gauss and 100 mTorr (Fig. 7a), where the measured density increases more strongly with power that the model predicts. In the 100 mTorr case, the predicted ion densities are consistently high by about a factor of two. At lower pressures, there is good agreement in scaling at all values of power and magnetic field, and for low magnetic field cases pretty close agreement in the magnitude of n.

We believe this agreement between model and experiment is evidence that the basic modeling approach is sound and includes the essential physics. We believe it can lead to a predictive model when such features as non-homogeneous sheaths and more accurate electron transport and ionization models are used. In addition, a self-consistent, inhomogeneous sheath model needs to be used for stochastic heating[6].

We gratefully acknowledge the support of NSF Grant ECS-8517363, a Gift from Applied Materials, a State of California MICRO Grant, and DOE Grant DE-FG03-87ER13727.

REFERENCES

1. Wolf, S. and R.N. Tauber, *Silicon Processing for the VLSI Era*, Volume 1, Lattice Press, 1986.

2. Manos, D.M. and D.L. Flamm, *Plasma Etching — An Introduction*, Academic Press, New York, 1989.

3. Keller, J. H. and W. B. Pennebaker, *IBM J. Res. Rev., 23, 3 (1979).*

4. Chapman, B., *Glow Discharge Processes*, John Wiley & Sons, 1980.

5a. Godyak, V.A., *Sov. J. Plasma Phys.* 2, 78 (1976).

5. Godyak, V.A., *Soviet Radio Frequency Discharge Research*, Technical Report, Delphic Associates, Virginia, 1986.

6. Lieberman, M. A., *IEEE Trans. Plasma Sci.* 16, 638 (1988).

7. Lieberman, M. A., *IEEE Transactions on Plasma Science* 17, 338 (1989).

8. Misium, G. R., A. J. Lichtenberg, and M. A. Lieberman, *J. Vac. Sci. Technol. A* 7, 1007 (1988).

9. Lieberman, M.A., *J. Appl. Phys.* 65, 4168 (1989).

10. Lieberman, M.A. and S.E. Savas, *J. Vac. Sci. Technol. A* 8, 1632 (1990).

11. Laframboise, J.G., UTIAS Report No. 100 (Institute for Aerospace Studies, University of Toronto, 1966), equation 14.2 and Fig. 40.

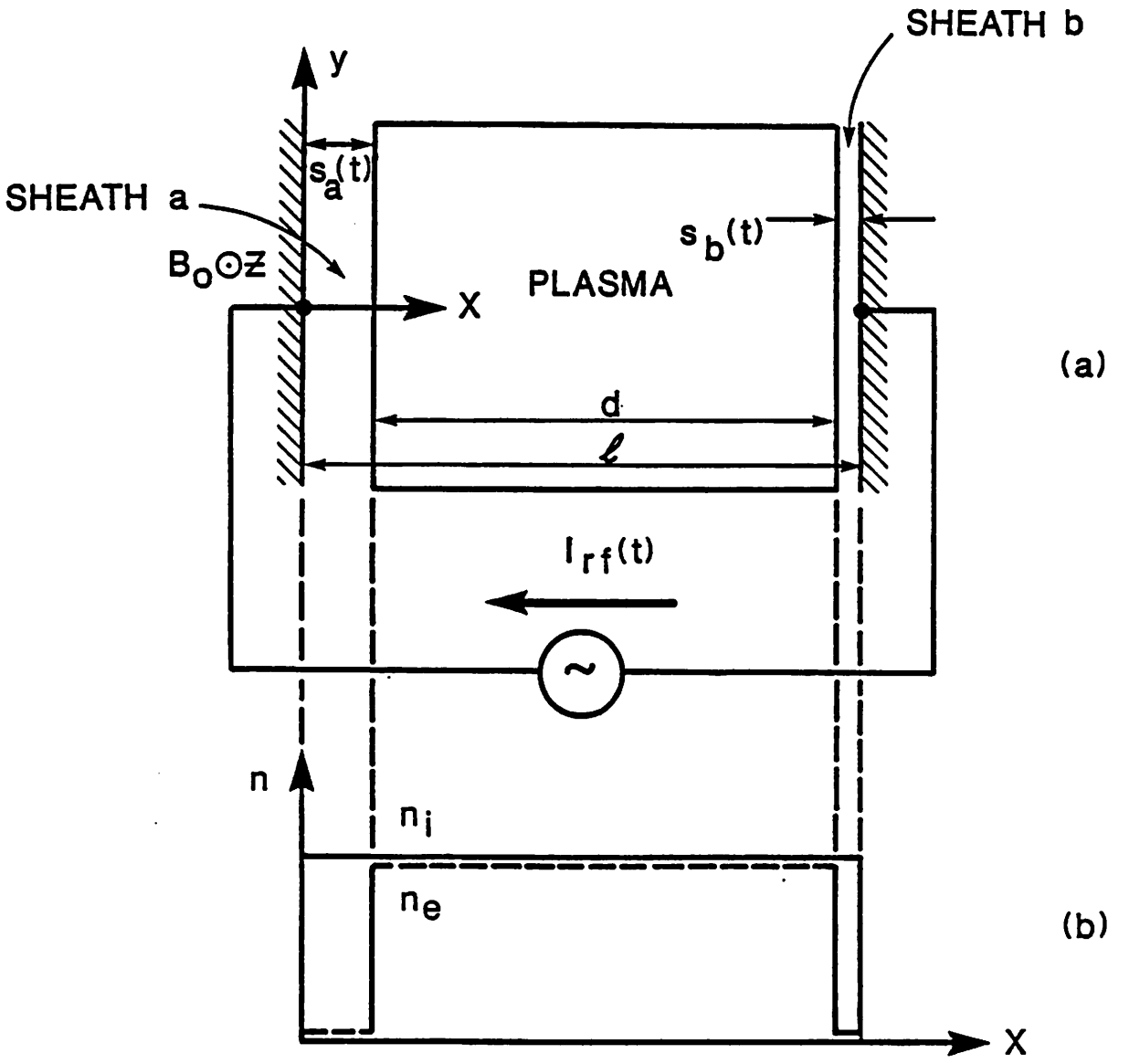

Figure 1. Model of a symmetric, plane parallel, magnetically enhanced capacitive r.f. discharge.

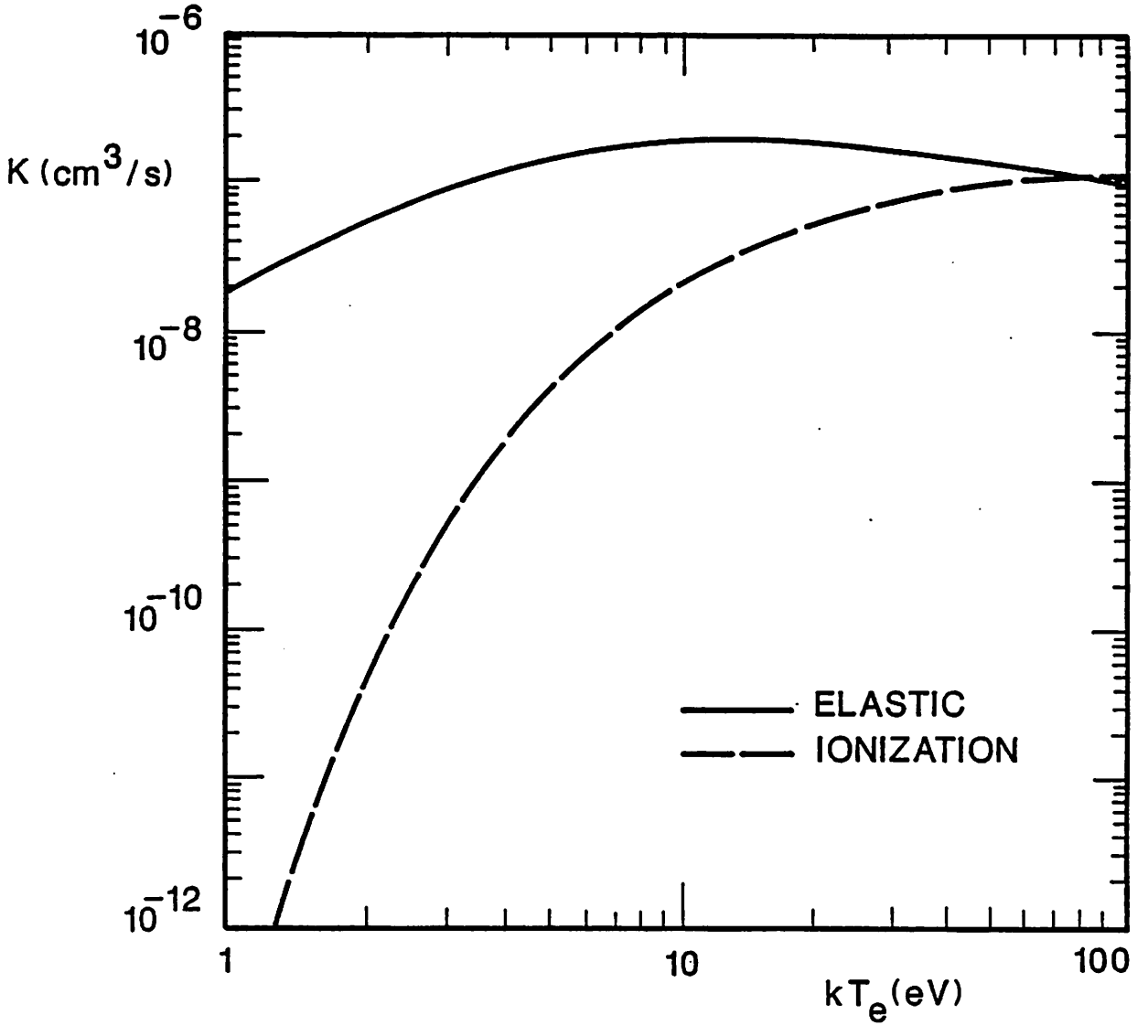

Figure 2. Rate constants for elastic scattering and ionization for electrons in argon gas.

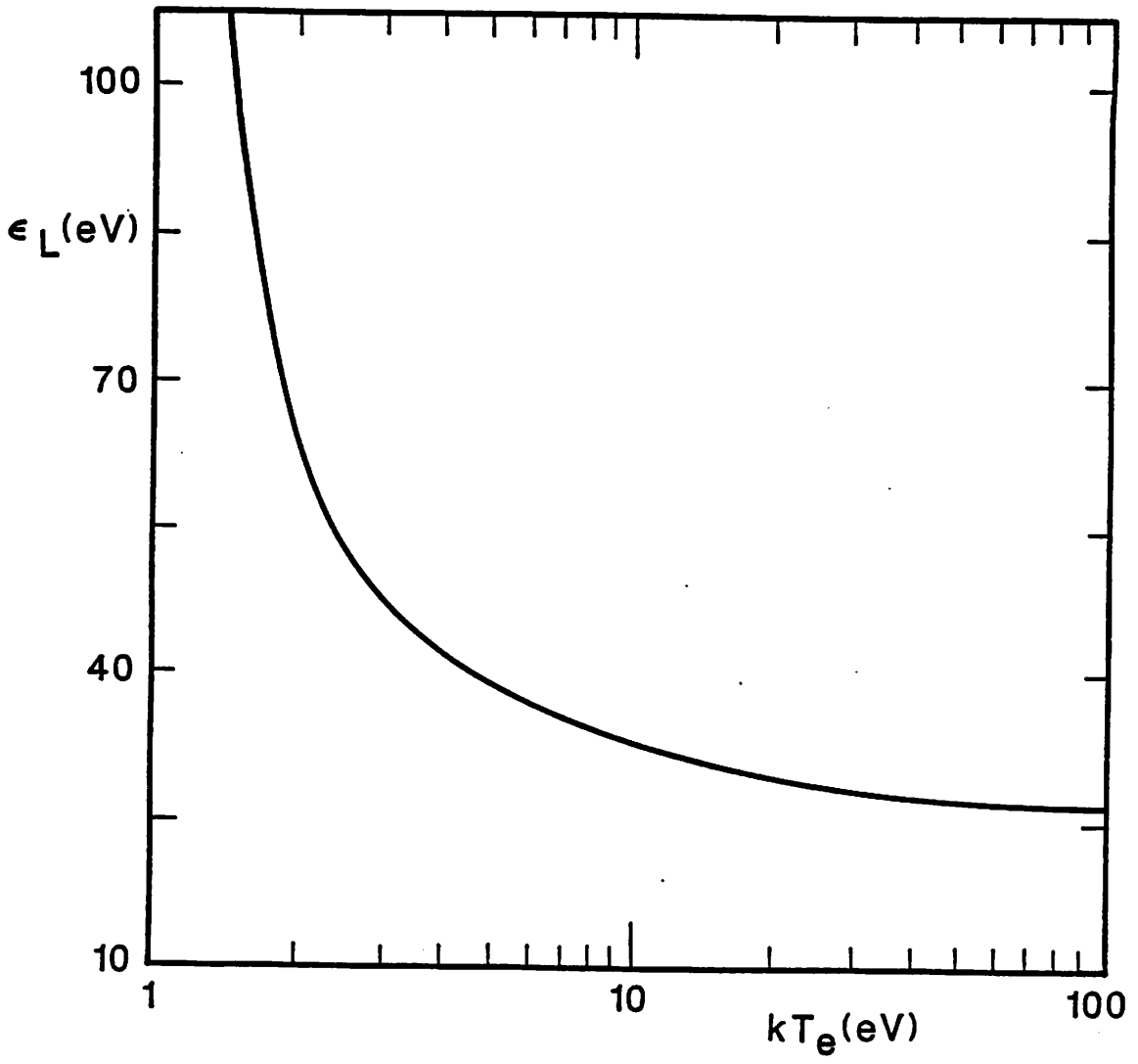

Figure 3. Mean energy ε_L required from an electron in order to create one electron-ion pair.

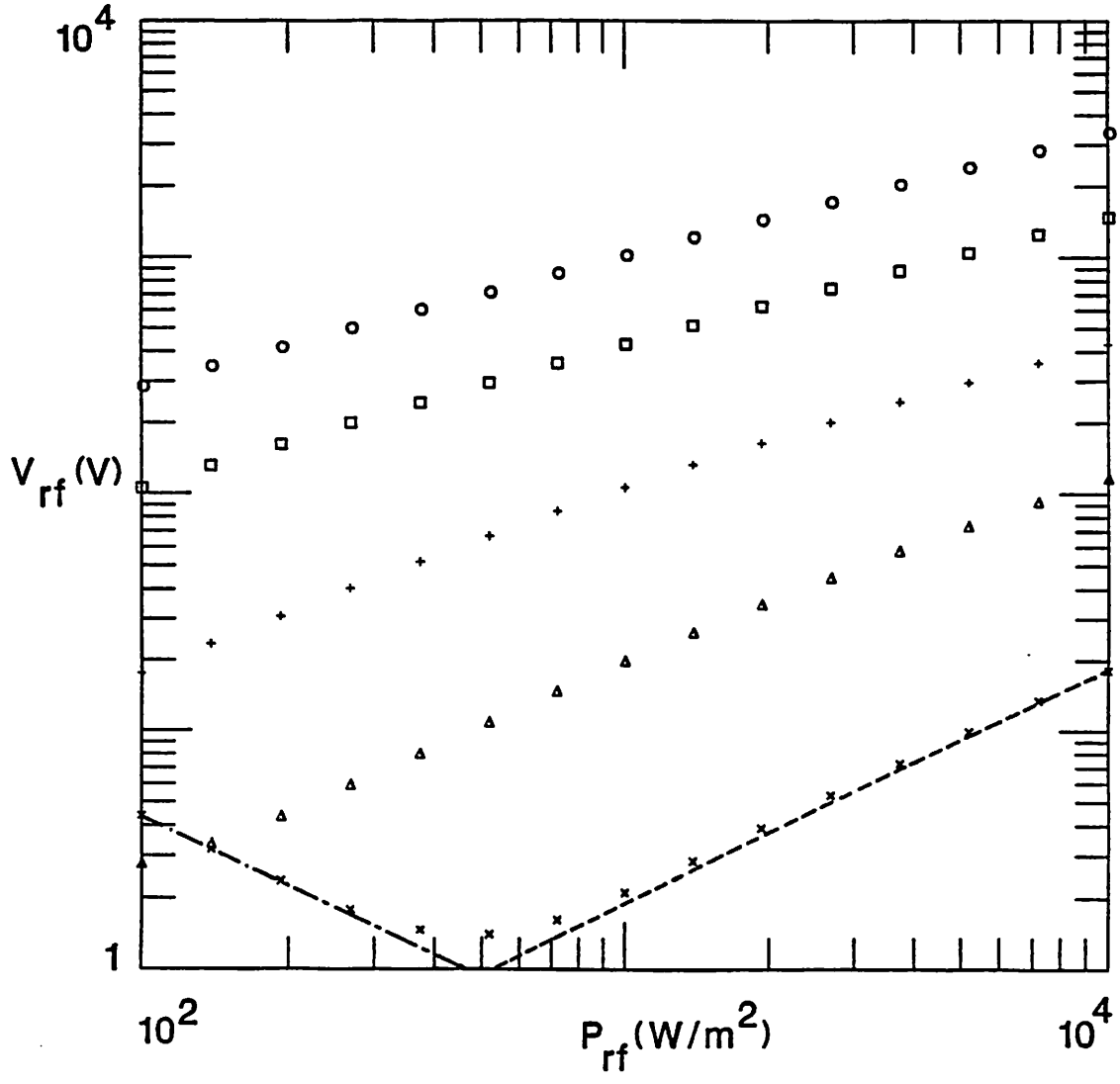

Figure 4. RF discharge voltage V_{rf} (a), ion density n (b), electron oscillation amplitude s_0 (c), and stochastic heating power per unit area P_{stoc} (d) for a 3 mTorr argon plasma 10 cm in length, for a range of r.f. power densities. Magnetic field values for the points are given by: O = 10 gauss, □ = 30 gauss, + = 100 gauss, Δ = 300 gauss, and × = 1000 gauss.

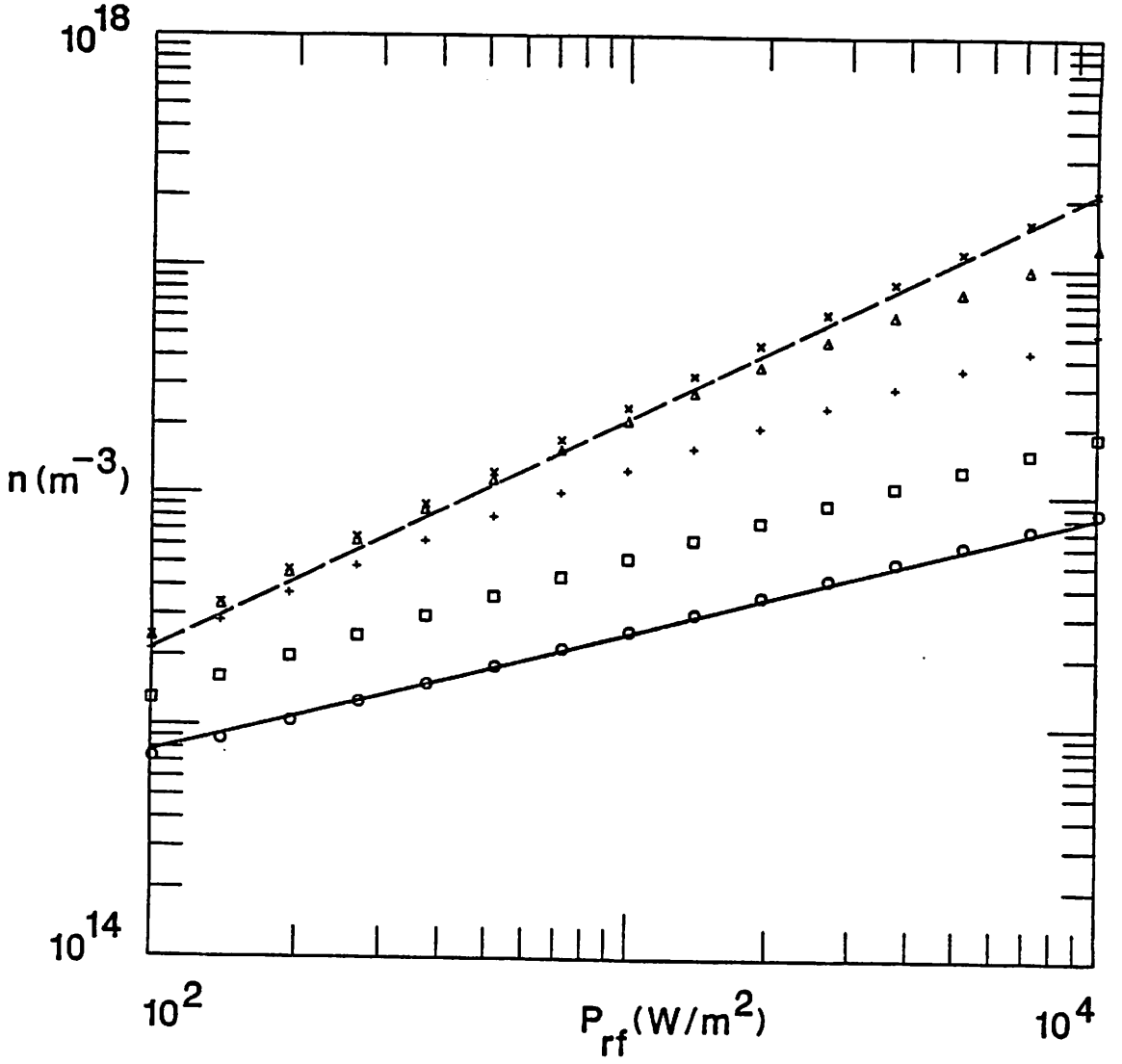

Figure 4b

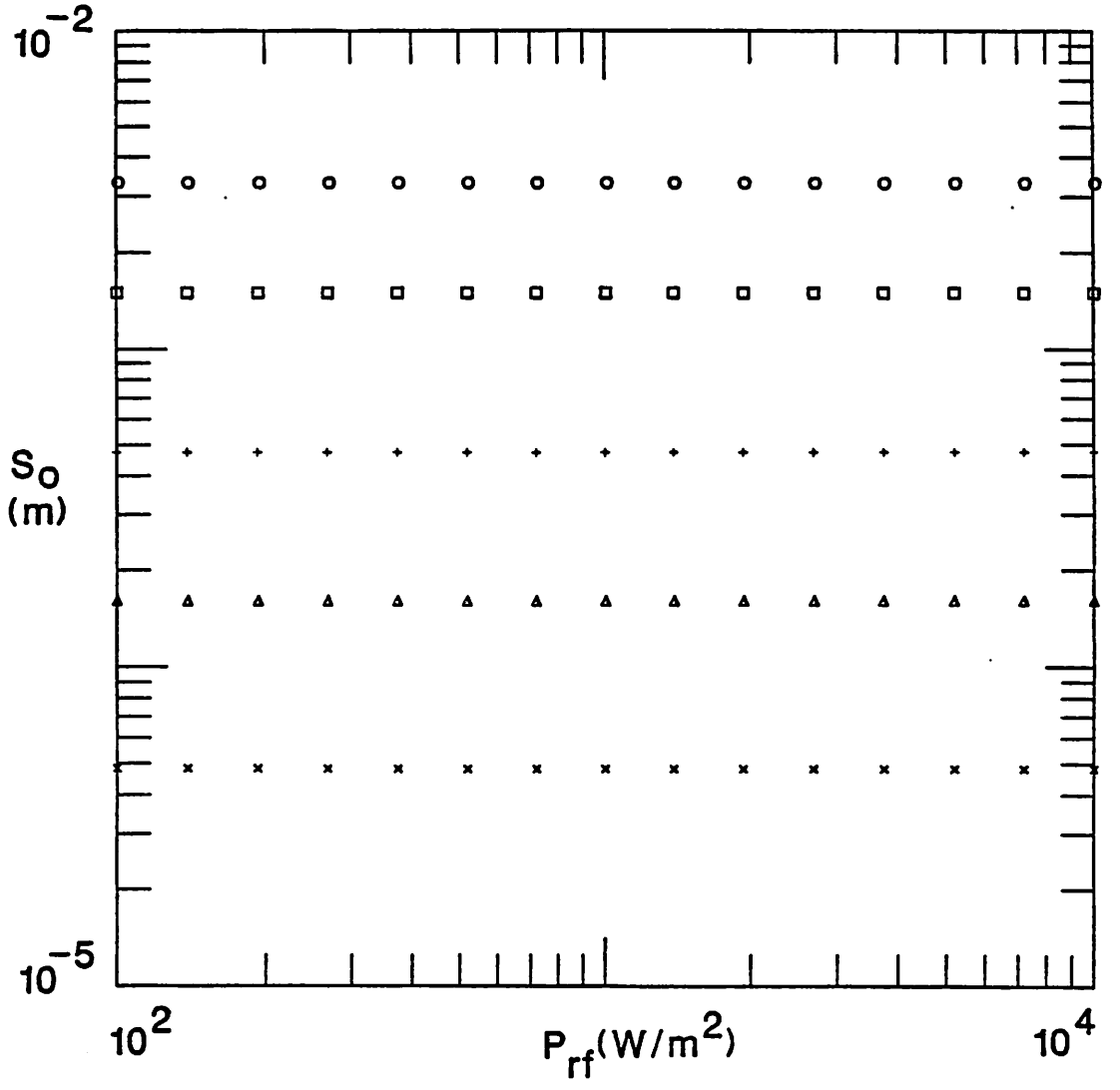

Figure 4c

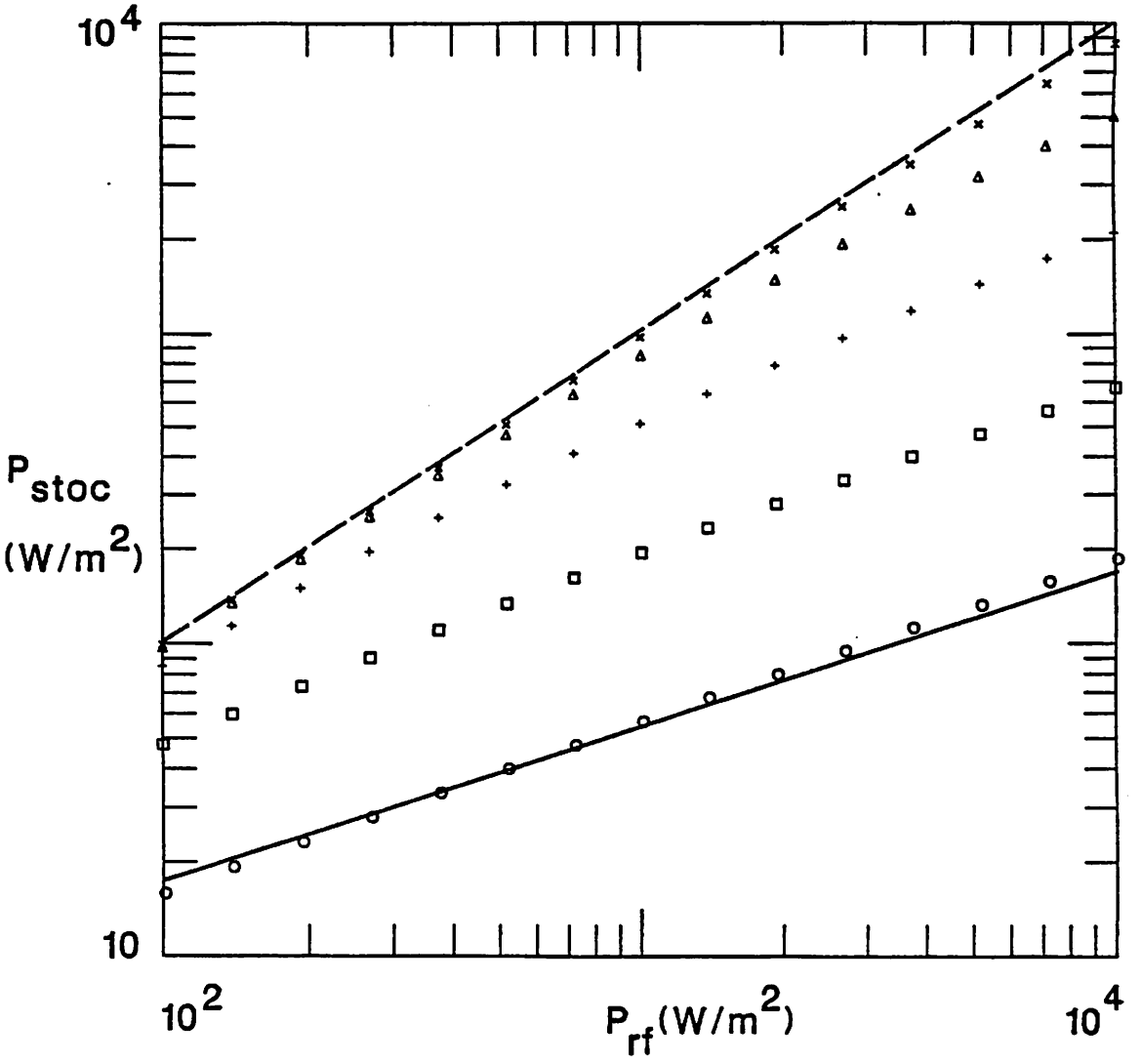

Figure 4d

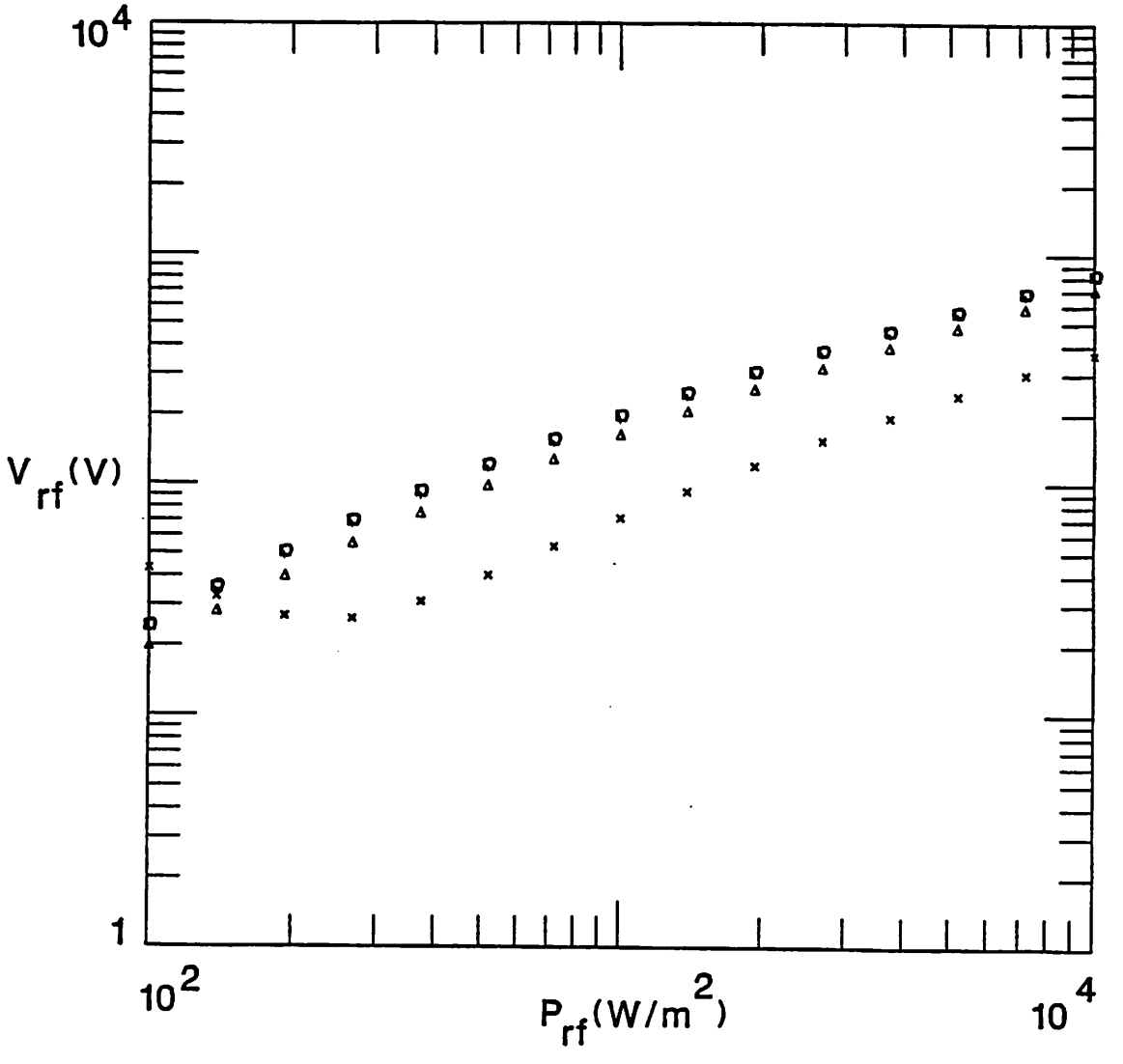

Figure 5. RF discharge voltage V_{rf} (a) and ion density n (b) for a 300 mTorr argon plasma 10 cm in length, for a range of r.f. power densities. Magnetic field values for the points are given by: O = 10 gauss, □ = 30 gauss, + = 100 gauss, Δ = 300 gauss, and × = 1000 gauss.

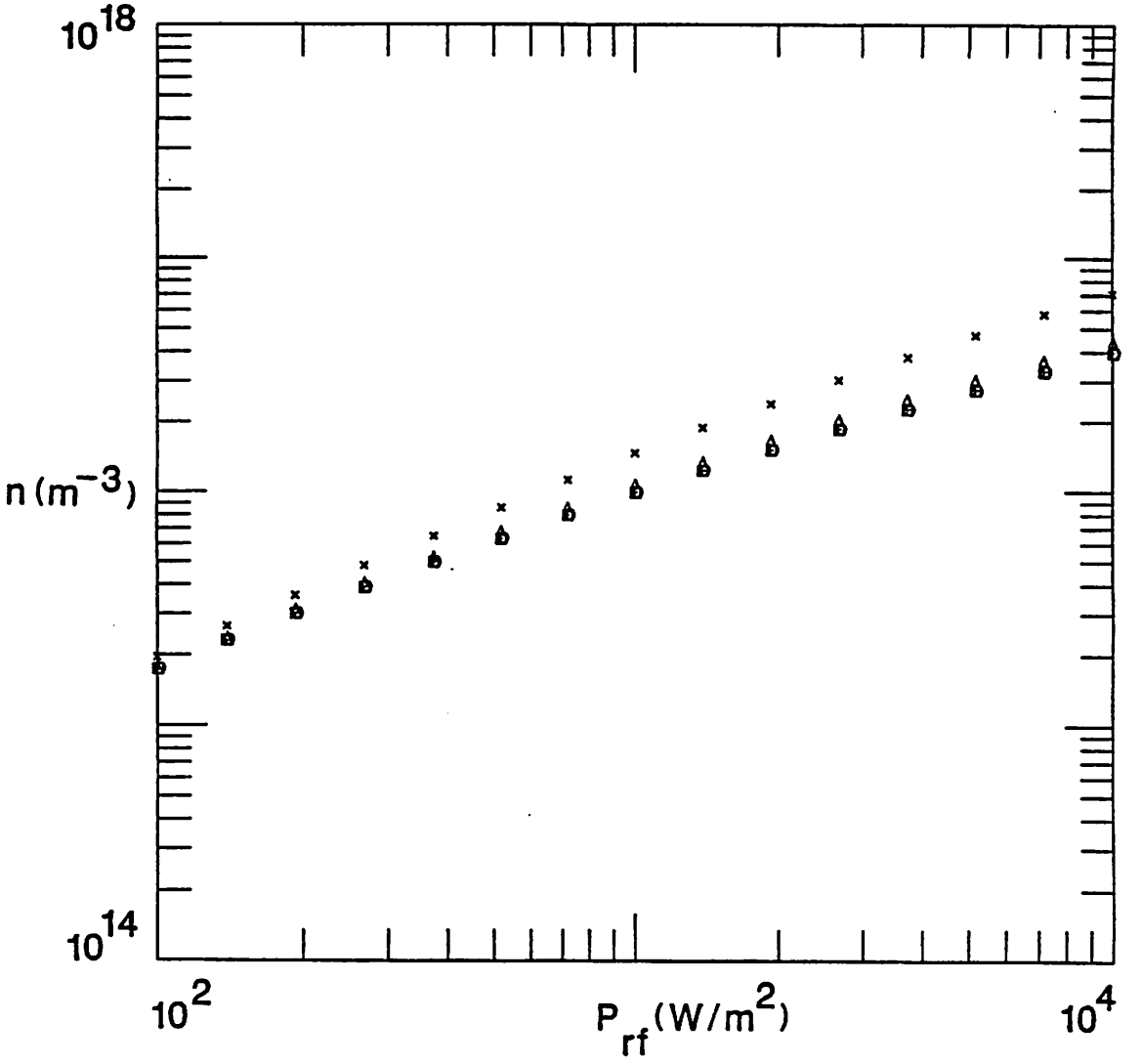

Figure 5b

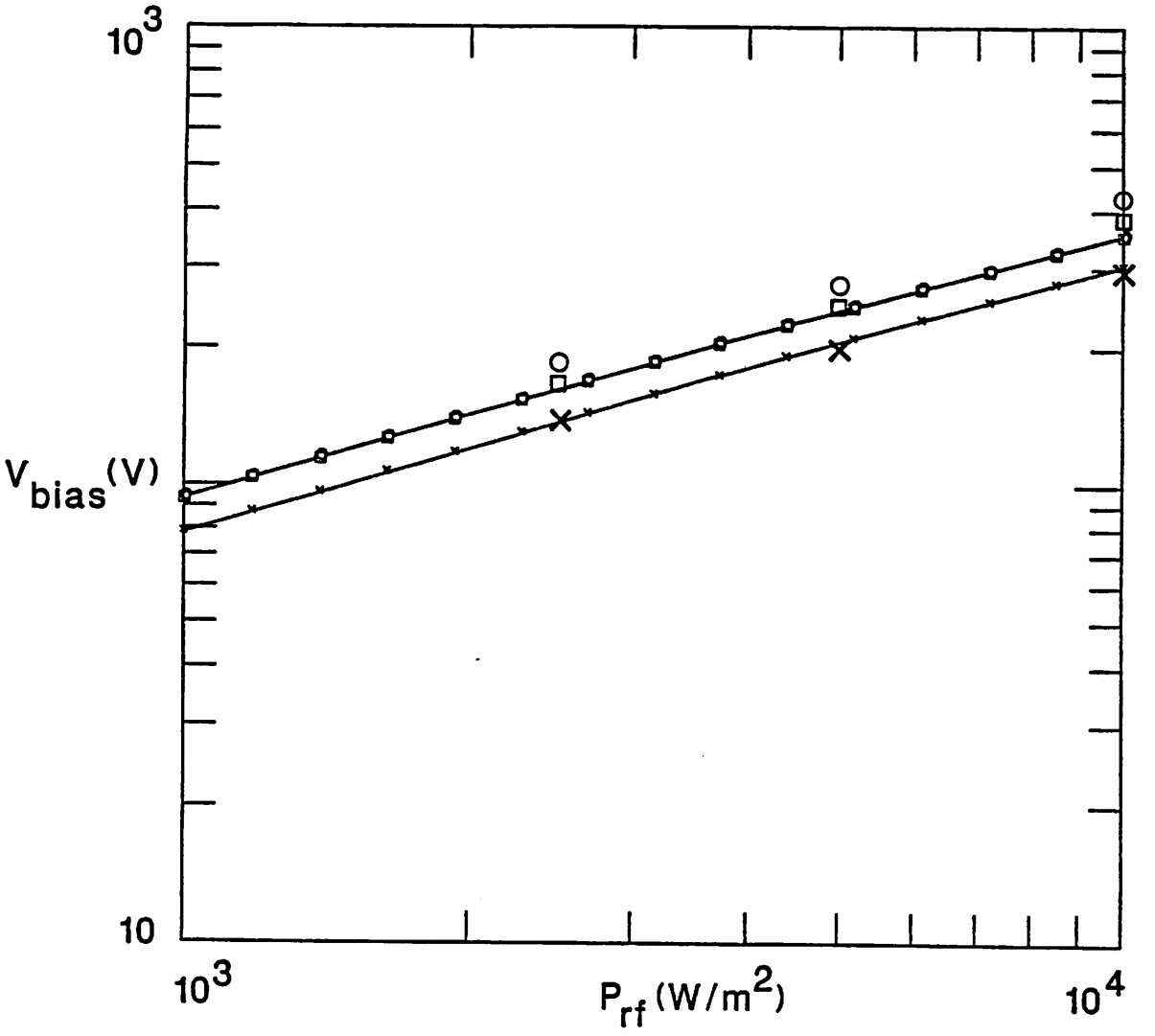

Figure 6. Bias voltage V_{bias} versus P_{rf} for magnetic fields of 10 gauss (○), 30 gauss (□) and 100 gauss (×). The small symbols connected by solid lines are the model results, and the large symbols are the corresponding measured results. (a) 100 mTorr; (b) 30 mTorr; (c) 10 mTorr.

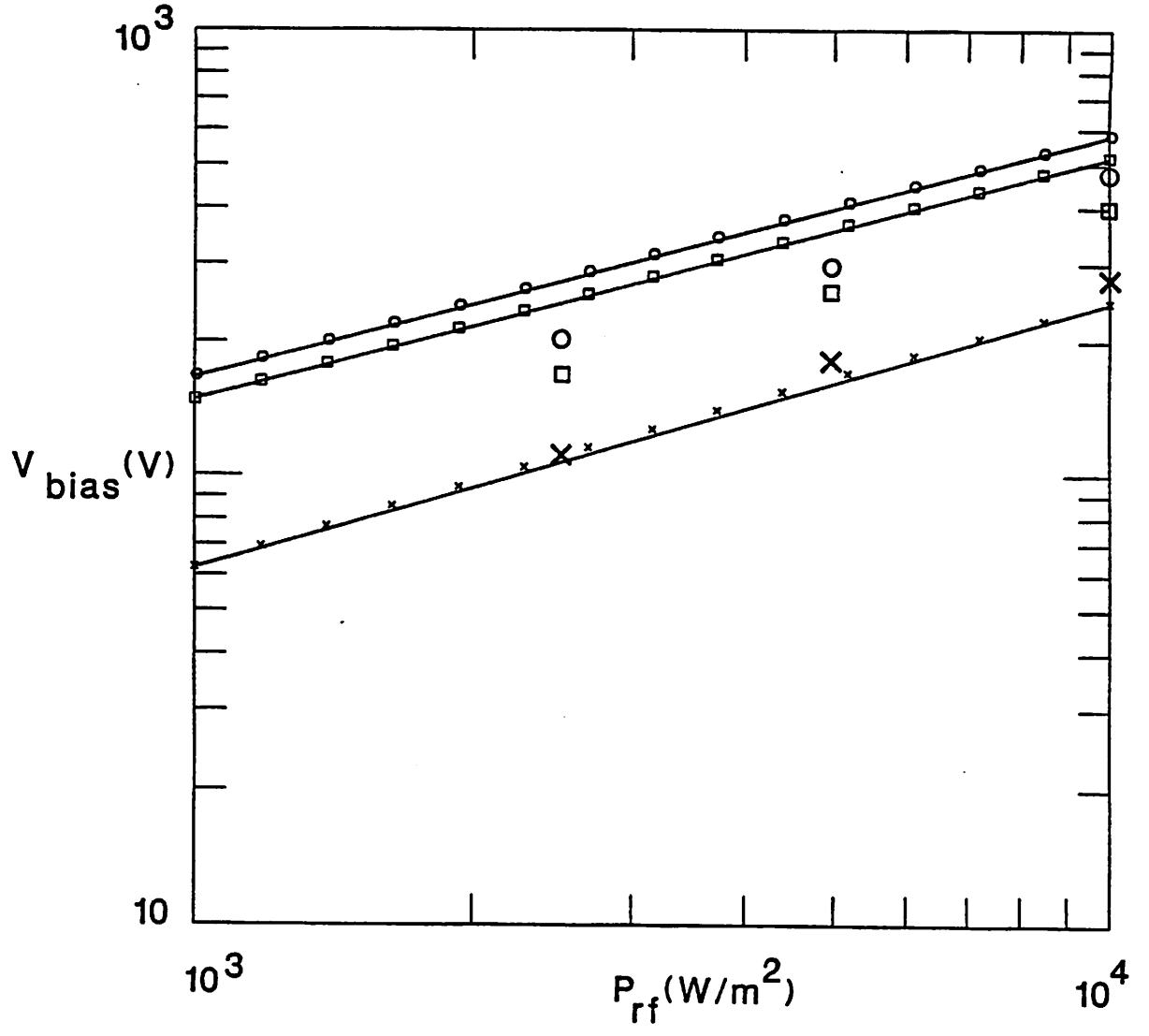

Figure 6b

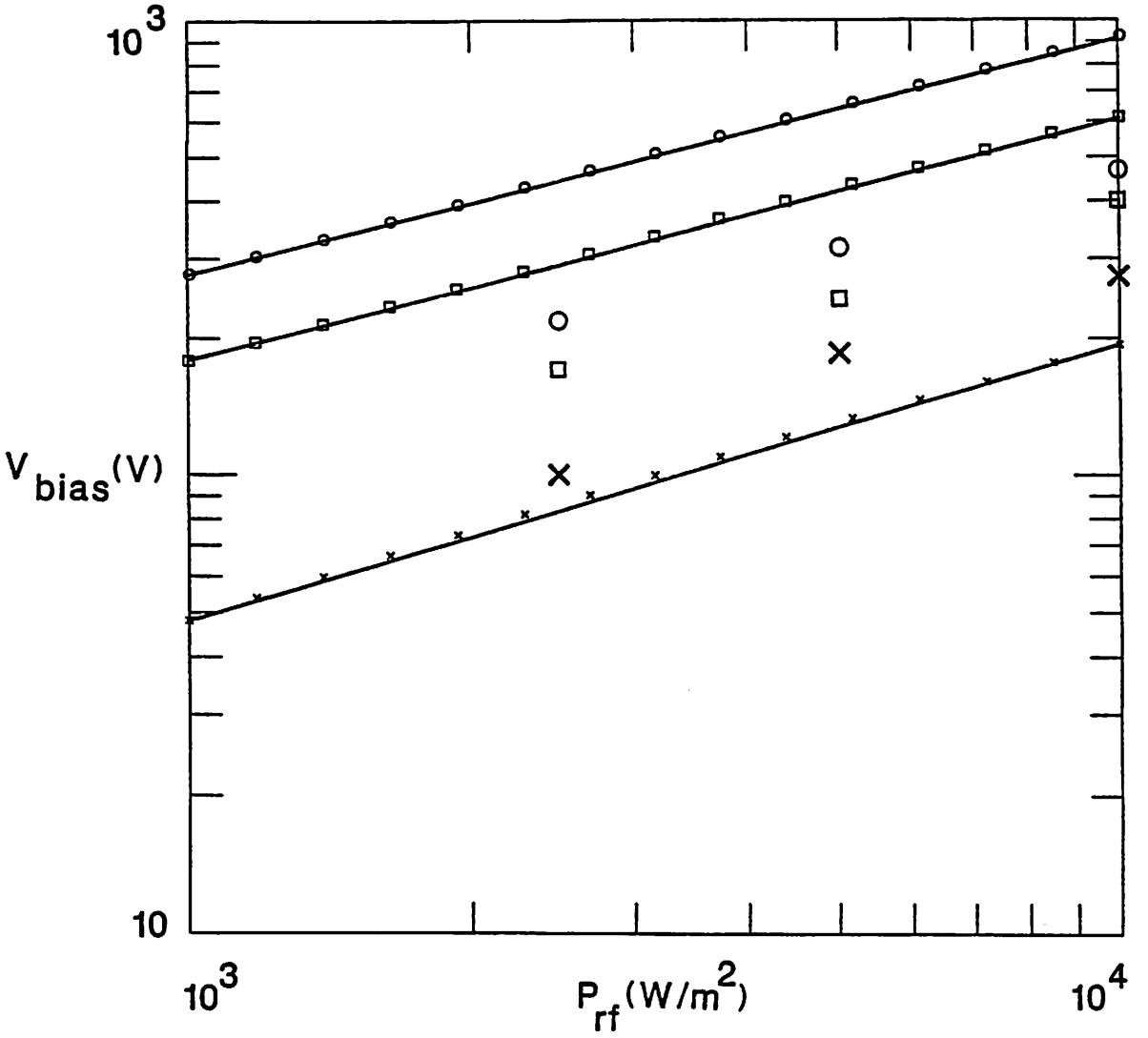

Figure 6c

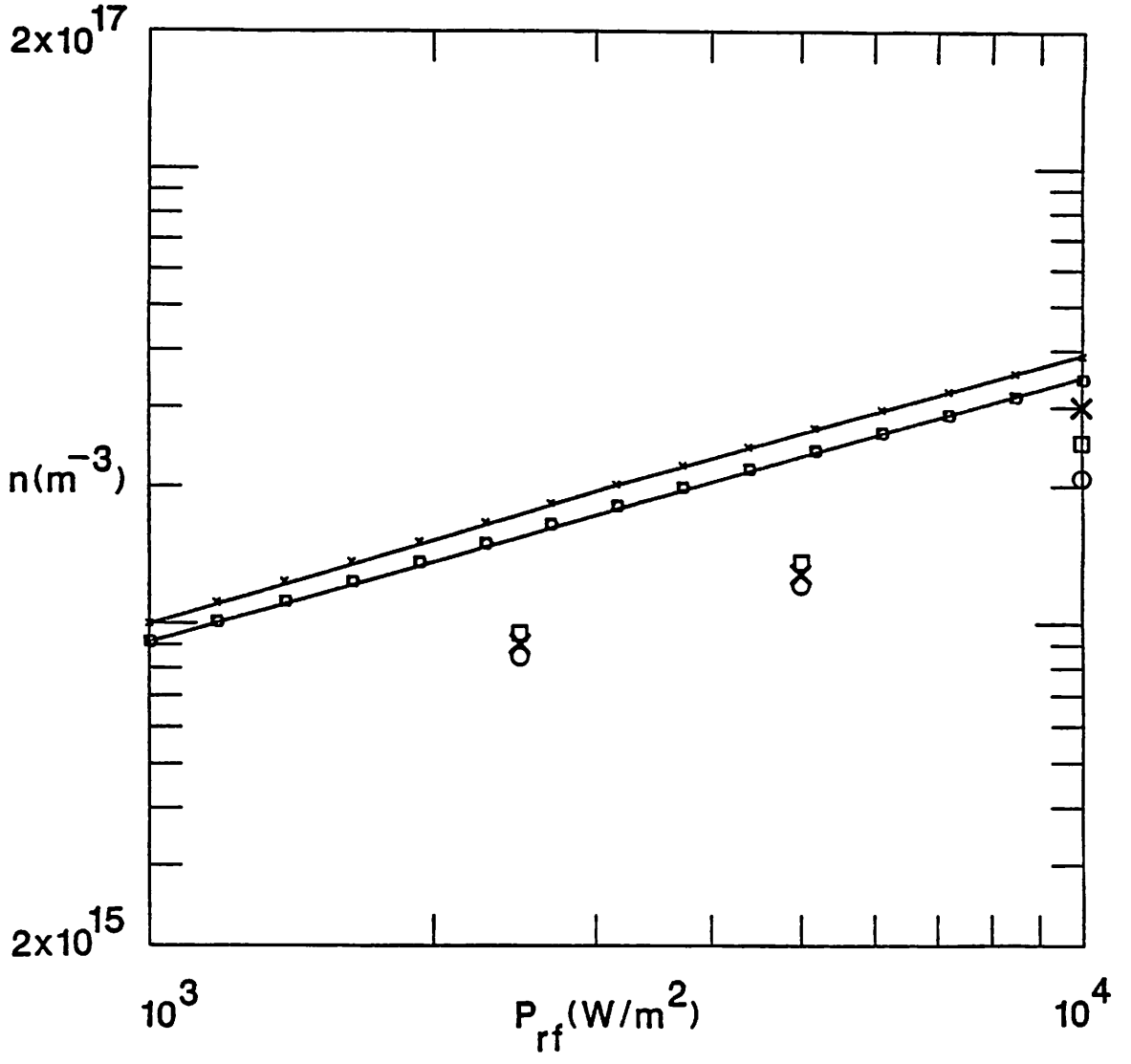

Figure 7. Ion density n versus P_{rf} for magnetic fields of 10 gauss (○), 30 gauss (□) and 100 gauss (×). The small symbols connected by solid lines are the model results, and the large symbols are the corresponding measured results. (a) 100 mTorr; (b) 30 mTorr; (c) 10 mTorr.

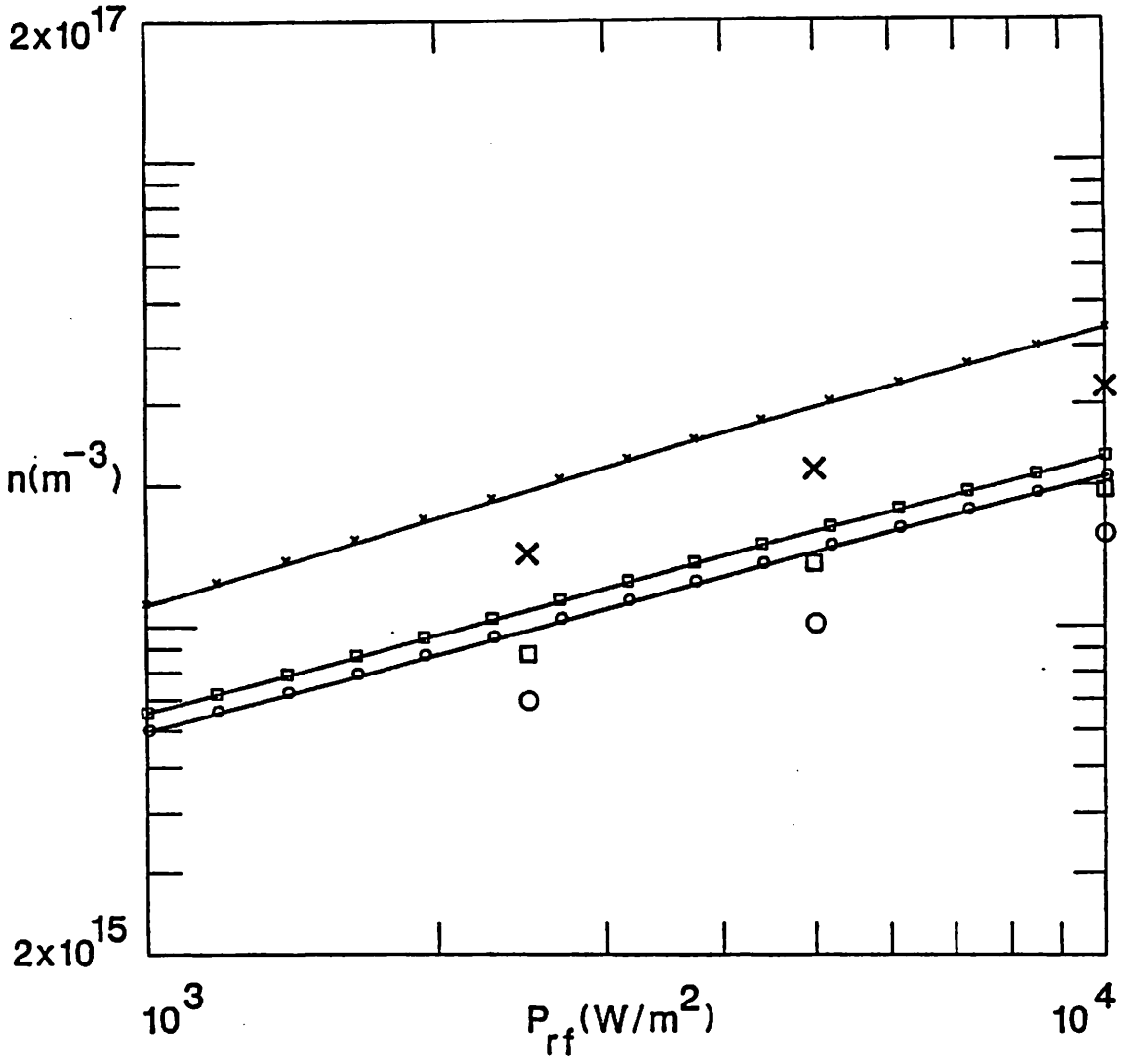

Figure 7b

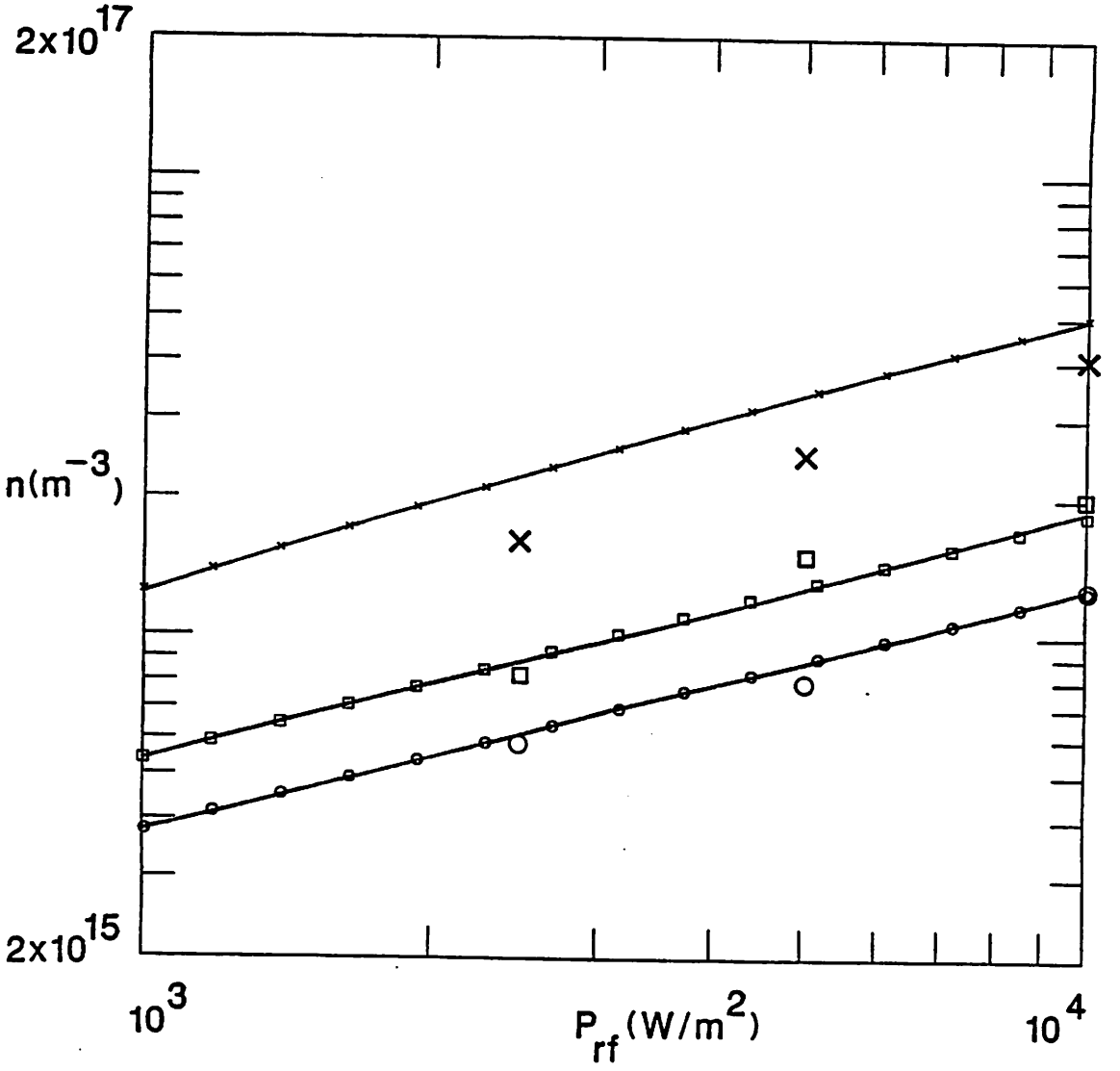

Figure 7c